Haq, B.U., and Ogg., J.G., 2024, Retraversing the highs and lows of Cenozoic sea levels: GSA Today, https://doi.org/10.1130/GSATG593A.1.

Supplemental Material

Supplemental Text S1. Further discussion of topics in main paper, rationale for refining ages of depositional surfaces, and additional documentation sources.

Figure S1. Composite Cenozoic depositional sequences and eustatic sea-level variations.

Supplemental Material for:

Retraversing the Highs and Lows of Cenozoic Sea levels

Bilal U. Haq[1] and James G. Ogg[2]
[1] Smithsonian Institution, Washington DC, and Sorbonne University, Paris, France
[2] Chengdu University of Technology, Chengdu, China and Purdue University, West Lafayette, Indiana

1. Introduction

In this online supplemental section of the paper we reconsider several issues that we could not discuss in detail in the main body of the paper due to space limitations. In addition, we also discuss the rationale for refining the ages of the depositional surfaces (on which the sea-level curves are based) with the help of oxygen isotopic data. For each Sequence Boundary (SB) and maximum flooding surface (MFS) that represent lows and highs in each depositional cycle, respectively, we describe the actual picks on the $\delta^{18}O$ curve. We also enumerate sources of the additional European and worldwide documentation for each SB.

2. Oxygen-isotopic ($\delta^{18}O$) data and issues with determining the amplitude of sea-level change

As discussed in the main text of the paper, in addition to deep-water temperature and ice volume on land, the values of benthic foraminiferal $\delta^{18}O_{sw,}$ are also affected by chemical dissolution products of the seafloor rocks, largely basalts accreted on the seafloor or along the mid ocean ridges. However, chemical weathering is a relatively slow process and is considered to be trivial over the duration of the Cenozoic (Veizer et al., 1999, Jaffrés et al., 2007, Pearson, 2012). Other complications, though also relatively minor, that can modify the $\delta^{18}O$ values are the fractionation due to vital effects and local salinity variations (the evaporation-precipitation and fresh-water inflow effects) that may have to be corrected for in planktonic forams for surface water temperature estimates (see, Pearson, 2012). The benthic oxygen-isotopic record is fraught with many inherent as well as external uncertainties that become progressively more challenging to resolve as the record gets older. Some of the inherent complications include: intra-specimen variability of up to 2‰ (which would be otherwise interpreted as ~200 m of sea-level change) that has been shown to exist in tests of the same species (Killingly et al., 1981); diagenetic alterations through post-depositional dissolution, precipitation of calcite cements from pore waters (including micro-recrystallization in carbonate tests); exposure to oxygen during storage (see, Pearson 2012). These factors can introduce significant sources of errors in our calculations if precision is the objective rather than deciphering the general trends.

Employing Mg/Ca ratios, with their potential for independently providing the necessary corrections for the bottom-water temperature component in the $\delta^{18}O_{sw}$ also have some issues. The connection between temperature and Mg/Ca composition is not well understood, but it is thought to involve the degree of assimilation of Mg in the calcitic tests of the benthics during the vital functions of the organism that is temperature dependent (Rosenthal et al., 1997). This has been ascertained by several lab studies and calibrations have been produced and refined (see, e.g., Lea et al., 2002). Nevertheless, teasing out temperature information from Mg/Ca is assumption dependent and can vary widely (Cramer et al., 2011). Dawber and Tripati (2011) point out that there is considerable variance between values determined by different models and approaches, e.g., from fluid inclusions in salt crystals (Horita et al., 2002), ridge spreading rates (Stanley and Hardie, 1998) or cation fluxes (Wilkinson and Algeo, 1989).

Then there is also the cognizance that Mg/Ca ratios do not always express the prevailing benthic paleotemperatures, as exemplified by the observations of Lear et al. (2008). They noticed that at the Eocene-Oligocene transition, an obvious steep step cooling event and harbinger of major growth of ice sheets on Antarctica, which is clearly expressed by a sharp increase in $\delta^{18}O$ of benthic foraminifers, does not always show up in the Mg/Ca record. These authors ascribe this to the saturation-state effect on benthic foraminifera at deep-water sites that were below the calcite compensation depth (CCD). They go on to show results from well-preserved samples above the CCD and find a ~2.5°C shift indicated by Mg/Ca values. This implies that Mg/Ca records generated at deep sites below the CCD cannot be taken at face value. These anomalies make isolating an accurate measure of the ice-volume component from the isotopic data extremely challenging.

We discussed the issue of the progressive depletion of developing ice sheets with respect to ^{18}O in the main body of the text, and how it makes calculating a mean $\delta^{18}O$ values of ice sheets impractical if previous ice sheets do not melt completely. Two examples where substantial melting of Antarctic and Greenland ice was inferred from stable shoreline studies are: 1) in mid Pliocene where there is an interpreted high of up to 40 m above present-day mean sea level (PDMSL), e.g., Dowsett and Cronin (1990); Kaufman and Brigham-Grette (1993); and 2) in the mid Pleistocene during Marine Isotope Stage 11: ~20 m higher than PDMSL (Hearty et al., 1999; Olson et al., 2009). However, as shown by Raymo et al (2011) and Raymo and Mitrovica (2012), when these values are corrected for post-glacial crustal subsidence along the coastlines in question, it reduced the sea-level rise estimates considerably that suggest less than full melting and partial survival of the ice fields during the interglacials.

3. Third-order sequences vs orbital cycles: a potential linkage?

One often-posed question is why do our sequence-stratigraphic analyses capture the multiples of Milankovitch-scale cycles in some intervals and not in others? In our experience the degree of resolution in a stratigraphic section is clearly a function of the prevalent sedimentation rates: when the sediment accumulation rates are high we start seeing more higher-frequency (400-100 Kyr) cycles within the third-order cycles, which implies that the two are connected. In the typical continental margin sequences (away from the point-sourced areas of river deltas with their thick pile of sediments) sedimentation rates are moderate to low, allowing a lower resolution in which only the third-order sequences can be identified. The long period modulations of the orbital cycles, i.e., 1.2 Myr (obliquity) and 2.4 Myr (eccentricity) have been documented in $\delta^{18}O$ and $\delta^{13}C$ records in the Cenozoic (e.g., Wade and Pälike, 2004; Pälike et al., 2006; Liebrand et al., 2016; Boulila, 2019; Kocken et al., 2019). Our sea-level record shown here (Fig. S1) also indicates several intervals where these periodicities dominate (with short intervals that deviate from such cyclicity, which can be attributed to either local or far-field tectonics, since the third-order cycles are recording these influences as well):

Interval 1: From 14.6 Ma (uppermost Burdigalian) through 23.03 Ma (Oligocene-Miocene transition) there are six cyclic sequences of 1.0 Myr (NBu3-NBu4), 1.1 Myr (NBu2- NBu3), 1.0 Myr (NBu1-NBu2), 1.2 Myr (NAq3-NBu1), 0.8 Myr (NAq2-NAq3) and 1.53 Myr (NAq1-NAq2). The s4–s3 obliquity/tilt cycle is quasi-periodic, its periodicity in the Cenozoic in La2004 astronomical model for example, ranges from 1.0 to 1.4 Myr. Thus, except for sequence NAq2-NAq3 the duration of all other sequences fall within the frequency band of s4–s3 orbital cycle.

Interval 2: From 39.0 Ma (mid-Bartonian) through 50.0 Ma (late Ypresian) there are five cyclic sequences of 1.5 Myr (PLu4-PBa1), 2.0 Myr (PLu3-PLu4), 2.6 Myr (PLu2-PLu3), 1.7 Myr (PLu1-PLu2) and 2.2 Myr (PYp8- PLu1). Durations of sequences PLu3- PLu4, PLu2-PLu3, and PYp8-PLu1 fall in the frequency band of g4–g3 orbital cycle. If we consider the average duration of the five sequences over the 39-50 Ma interval, we find a 2.2 Myr cyclicity, which is close to the mean period of g4-g3 eccentricity cycle.

Other intervals that show cycle duration in the 400 Kyr bands are: PYp6-PYp7, PYp5-PYp6, PTh2-PTh3, PSe1- PSe2. This periodicity becomes discernable when sediment accumulation rates were high. It is therefore reasonable to conclude that the Cenozoic third-order depositional sequences are dominantly modulated by the orbital cycles and are thus, also a function of climatic variations, with tectonics most likely playing an important but secondary role.

4. Fine-tuning of sequence boundaries and maximum flooding surfaces

As discussed in the main body of the paper, $\delta^{18}O$ trends have aided us in refining the age picks for SBs and MFSs and the essentially global signal contained in the isotopic data permit age assignments that would be globally acceptable. Although some ephemeral ice on Antarctica is suspected as far back as late Cretaceous (see, e.g., Matthews and Poore, 1980, Matthews, 1984, Miller at al., 2005; Haq 2014), substantial ice sheets began in the mid Eocene, which allows us to use oxygen-isotopic trends to refine the ages of depositional surfaces for much of the Cenozoic. The relatively prominent enrichment and depletion episodes of $\delta^{18}O$ are considered as indicators of growth and decay of ice sheets at least since the mid Eocene, and prior to that as major cooling and warming trends in climate. There are a number of relatively recent and useful $\delta^{18}O$ compilations of Cenozoic available (e.g., Zachos et al., 2001; Cramer et al., 2009; Veizer and Prokoph, 2015; Miller et al., 2020, among others). However, we have used the Westerhold et al.'s (2020) Cenozoic stack for its completeness, and because much of it is astronomically tuned.

4.1 *Age Model of Sequence Boundaries and Maximum Flooding Surfaces*

In this major reappraisal of the Cenozoic eustasy the chronological positioning of the Paleogene and Neogene SBs (mostly 3rd-order sequences, ranging from ~2.5 to 0.5 Myr in duration), as in the original works on which this revision is based (Haq et al., 1987, 1988, Hardenbol et al., 1998), are primarily picked on the basis of biostratigraphic criteria, and in addition, where possible, fine-tuned by calibration with oxygen isotopic data, using the $\delta^{18}O$ synthesis of Westerhold et al (2020). The Quaternary SB ages (4th & 5th-order sequences, >0.5 Myr in duration; mostly ranging from ~400 to 100 Kyr), on the other hand, are primarily picked on isotopic basis, as the biochronological criteria often cannot resolve such finer time scales.

Our rationale for using the $\delta^{18}O$ trends for refining the ages of the SBs and MFSs is quite simply that the prominent trends in enrichment of $\delta^{18}O$ vs its deficit are partial indicators of waxing vs waning of continental ice sheets since the Lutetian (or major bottom-water cooling vs warming trends in the pre-mid Eocene). The beginning of the relatively rapid cooling trends, when they occur close to the biostratigraphically dated SBs, help us refine the ages of the those boundaries, while the warming trends aid in the ascertaining the MFSs that present greater dating challenge when dated on biostratigraphy alone (also discussed in the main body of the paper).

Sequence boundaries (SB) and maximum flooding surfaces (mfs) that alternate on the cycle charts (Figs. 1, 2 in the main text, and Fig. S1 here) are listed here in chronological order, from younger to older. They are alpha-numerically designated following the convention used by Hardenbol et al. (1998), however, the letter P (for Paleogene), N (for Neogene) and Q (for Quaternary) are added before the alphanumeric designations (e.g., for the event NTo1, the letter "N" denotes Neogene, letters "To" are the first two letters of Tortonian Stage, and the digit "1" indicates the SB number 1 that is the lowest within the Tortonian interval). This makes such designations unique and avoids confusion with similar alphanumeric abbreviations in other periods. We followed the same system of designation also in the updates of the sea-level curves for the Mesozoic subdivisions (see Haq, 2014, 2018a and 2018b, for Cretaceous, Jurassic and Triassic, respectively). The alphanumeric designation of the MFSs is the same as the preceding (older) SB, with the letters "mfs" added after the identifiers to distinguish them from the SBs. [Note: The concept of MFS is best developed on the transgressive shelf (or on the inundated inland seas). In a few cases, when the

precise age of the MFS cannot be ascertained or refined using $\delta^{18}O$ trends, it is schematically placed at the mid point of the sequence cycle, i.e., middle of the two sequence boundaries. In practice, the timing of when the level of the MFS is reached within a sequence cycle is a function of the rate of local (eurybatic) sea-level rise (transgression over the shelf) that competes with the rate of sediment supply to the system to determine when the transgressive trend will change to a regression (after reaching a maximum flooding point), which will vary from place to place. The age of the MFS will, likewise, be somewhat time-variable from one location to the other. Thus, the convention of placing it at the mid-point of the cycle, when there is no indication of a prominent change in the trend gleaned from the $\delta^{18}O$ data.

For the Quaternary SBs and MFSs that are younger than mid-Calabrian (i.e., younger than QCa 2 SB at 1.48 Ma) the main dating criteria are isotopic [i.e., they are tied to the Marine Isotopic Stages (MIS) identified on the $\delta^{18}O$ curve of Westerhold et al. (2020)]. Therefore, we have also added the MIS number to which they are calibrated (e.g., QMIS22, QMIS19 mfs, etc). The youngest SB that was caused by the withdrawal of the sea during the Last Glacial Maximum is designated as QLGM.

4.2 *Placement of boundaries and calibration to oxygen-isotopic curves*

In the list below the ages of the bases of chronostratigraphic boundaries (Stages) are followed by the alphanumeric designation of SB and MFSs. That are progressively older. The relative magnitude of the sea-level falls at the SBs are as follows: *Major >75 m; Medium 25-75m; Minor < 25 m).* A short description of the reason(s) why and where the positions of the boundaries are picked follows the alphanumeric designation below. All isotopic calibrations are made using the $\delta^{18}O$ composite of Westerhold et al. (2020).

Anthropocene (age of the base currently not agreed upon).

Ho-1 mfs – (?) (Major): A major marine transgression occurred at the onset of Holocene (~10 Kyr ago). However, the maximum flooding level (highest sea level) has not yet been achieved if we presume (as empirical hydrological data and various models indicate) that sea level will continue to rise into the future, largely through the rapid melting of the Greenland and Antarctic ice caps. The extant sea level during the current cycle is estimated to exceed the previous (Eemian) maximum highstand.

Holocene (age of the base 0.01 Ma)

QLGM - 0.033 Ma (Major): The Last Glacial Maximum is variously dated as commencing at 33 Kyr to 27.5 Kyr BP. The sequence boundary QLGM marks the onset of the LGM, within the marine isotope stage 2 (MIS 2) and is placed here at 0.033 Ma.

Late Pleistocene (age of the base 0.129 Ma)

QCh6(MIS5e) mfs - 0.12 Ma (Major): Placed at the onset of major interglacial MIS 5e (as calibrated through Westerhold et al. (2020), base of Emsian regional stage.
QCh6(MIS6) - 0.18 Ma (Major): Marks the onset of glacial MIS 6 (Illinoian/Saalian glacial)
QCh5(MIS7) mfs - 0.24 Ma (Medium): Marks the onset of initial pulse of interglacial MIS 7.
QCh5(MIS8) - 0.28 Ma (Major): Placed at the onset of glacial MIS 8.
QCh4(MIS9) mfs - 0.33 Ma (Major): Placed at the onset of interglacial MIS 9.
QCh4(MIS10) - 0.38 Ma (Major): Picked at the onset of glacial MIS 10.
QCh3(MIS11) mfs - 0.42 Ma (Major): Marks the onset of interglacial MIS 11.
QCh3(MIS12) - 0.47 Ma (Major): Occurs in the upper CNPL10 nanno Zone. Placed at the onset of

glacial MIS 12 on the Westerhold et al (2020) curve.
QCh2(MIS13) mfs – 0.50 Ma (Medium). Placed within the rapid change at ~0.51 Ma that peaks at ~0.49 Ma.
QCh2 (MIS 14) - 0.57 Ma (Medium). A relatively smaller amplitude glacial on the $\delta^{18}O$ curve, marking a rapid change before the peak, with the lowstand at 0.55 Ma
QCh1(MIS15) mfs - 0.62 Ma (Medium): Picked at the onset of (major) interglacial MIS 15 interval, the first major 100-kyr-spaced interglacial cycle on the $\delta^{18}O$ curve of Westerhold et al. (2020).
QCh1(MIS16) - 0.68 Ma (Major): Occurs in the mid-CNPL10 nanno Zone. Placed at the onset of glacial MIS 16, the first (major) ~100 Kyr-spaced glacial cycle.

Chibanian (age of the base 0.77 Ma)

QCa3(MIS19) mfs - 0.81 Ma (Major): Picked at the interglacial MIS 19 on the Westerhold et al ($\delta^{18}O$) curve.
QCa3(MIS22) - 0.90 Ma (Major): Occurs in the lower portion of CNPL10 nanno Zone. Placed at the onset of glacial MIS 22 is highest $\delta^{18}O$ interval in the combined MIS 22-24 cold event.
QCa2(MIS25) mfs - 0.95 Ma (Medium): Picked at the onset of interglacial MIS 25.
QCa2 - 1.5 Ma (Medium): Positioned near the mid-CNPL8 nanno Zone that marks the onset of glacial MIS 48, which is a (major) peak in $\delta^{18}O$ on the Westerhold et al. (2020) curve.
QCa1 mfs -1.60 Ma (Minor): Within the lower CNPL8 nanno Zone, interglacial MIS 57-55 (~1.64-1.59 Ma) appears to span an interglacial highstand,
QCa1 - 1.70 Ma (Medium): Placed at the base of CNPL8 nanno Zone that coincides with cold event MIS 60 event within a generally cooler interval of MIS 62 to MIS 58.

Calabrian (age of the base 1.8 Ma)

QGe2 mfs - 1.82 Ma (Medium): Placed within the CNPL7 nanno Zone, which also marks a warming trend across the Gelasian-Calabrian stage boundary. Fine-turned to coincide with warm MIS 65 event.
QGe2 - 2.15 Ma (Medium): Placed at the mid-PL6 foram and CNPL6(NN18) nanno Zones that marks the onset of (major) cold event MIS 82 (peak of higher $\delta^{18}O$) on the curve of Westerhold et al. (2020).
QGe1 mfs - 2.38 Ma (Medium): Placed at the base of PL6 foram and CNPL6 (NN18) nanno Zones. Positioned in the early part of interval with relatively warm (lower $\delta^{18}O$) average conditions on the curve of Westerhold et al. (2020).
QGe1 - 2.54 Ma (Major): Placed at the base of NN17 nanno Zone. The event marks the earliest significant Quaternary glacial event (MIS 100), with extremely high $\delta^{18}O$ peak (cold interval) on the curve of Westerhold et al. (2020).

Gelasian (age of the base 2.58 Ma) Base of Quaternary

NPi2 mfs - 2.58 Ma (Medium): Placed within the CNPL5 nanno Zone and at the Piacenzian-Gelasian boundary, marked by warm (low $\delta^{18}O$) peaks on the curve of Westerhold et al. (2020).
NPi2 - 2.73 Ma (Major): Occurs close to the CNPL4-CNPL5 nanno zonal boundary. Marks the onset of a major but brief cold event (positive peak in $\delta^{18}O$ on curve of the Westerhold et al. (2020)) during latest Piacenzian = MIS110/G6.
NPi1 mfs - 3.2 Ma (Medium): Picked at the rapid warming soon after the NPia1-SB cold event.
NPi1 - 3.3 Ma (Major): Placed in the mid-CNPL4 nanno Zone. Fine tuned to coincide with the onset of (major but brief) cold event (positive peak in $\delta^{18}O$ on the curve of Westerhold et al. (2020) in the

early Piacenzian = MIS M2

Piacenzian (age of the base 3.6 Ma)

NZa2 mfs - 3.6 Ma (Medium): Positioned at the Piacenzian-Zanclean boundary, which also marks the beginning of a warm interval (low $\delta^{18}O$) on the Westerhold et al. (2020) curve.
NZa2 - 4.15 Ma (Major): Occurs at mid-PL2 foram and upper NN14 nanno Zones, marking the onset of relatively cool interval (peaks of higher $\delta^{18}O$) on the Westerhold et al. (2020) curve.
NZa1 mfs - 4.35 Ma (Medium): Positioned near the middle of sequence. Coincides with two warm (low $\delta^{18}O$) peaks on the Westerhold et al. (2020) curve.
NZa1 - 4.6 Ma (Major): Placed at mid-CNPL2 (NN13) nanno zone. Coincides with beginning of slightly cooler (higher $\delta^{18}O$) interval on the Westerhold et al. (2020) curve, but the signal is not a significant one.

Zanclean (age of the base 5.33 Ma)
.
NMe2 mfs - 5.4 Ma (Major): Occurs near the base of CNM 20 (NN12) nanno Zone, just before Messinian/Zanclean boundary. Assigned to earliest part of shift in baseline to warmer (lower $\delta^{18}O$) levels on the curve of Westerhold et al. (2020).
NMe2 - 5.75 Ma (Major): Near beginning of Pl1 (N18/N19) foram and mid CNM19 nanno Zones. Fine-tuned to coincide with a pronounced cool (high $\delta^{18}O$) episode on the curve of Westerhold et al. (2020).
NMe1 mfs - 6.0 Ma (Medium): Placed at the base of CNM19 nanno and mid-M14 foram Zones, within a relatively warmer (lower $\delta^{18}O$) interval in mid-Messinian.
NMe1 - 7.2 Ma (Major): Occurs in the lower CNM17 nanno Zone, just after beginning of Messinian. Beginning of progressive cooling (decreasing $\delta^{18}O$) trend that continues to ~ 6.2 Ma on the curve of Westerhold et al. (2020).

Messinian (age of the base 7.25 Ma)

NTo1 mfs - 7.7 Ma (Medium): Occurs in the mid-CNM16 nanno Zone, which also marks the onset of warming (lower $\delta^{18}O$) trend on the curve of Westerhold et al. (2020).
NTo1 - 9.3 Ma (Medium): Occurs at mid-CNM14 nanno and mid-N16 foram Zones. Placed here at beginning of relative cool (higher $\delta^{18}O$) episode on the Westerhold et al. (2020) curve. However, the early part of this NTo1 sequence includes some similar episodes, such as the cool (high $\delta^{18}O$) peak at ca. 8.7 Ma.
NSe3-To1 transition mfs - 10.8 Ma (Major): The NSe3 event that almost straddles the Serravallian/Tortonian boundary extends into the Tortonian. The mfs within this sequence is placed at a pronounced shift from cool to warm (lower $\delta^{18}O$ peaks) on the Westerhold et al. (2020) curve.

Tortonian (age of the base 11.62 Ma)

NSe3 - 11.7 Ma (Major): This event almost straddles the Serravallian/Tortonian boundary, placed here at the base of M11/N14 foram and CNM7 nanno Zones. Mi-5 cooling event occurs just before the beginning of the Tortonian Stage.
NSe2 mfs - 12.2 Ma (Minor): Placed in the middle of CNM8 nanno Zone, within a interval of relatively warmer (higher $\delta^{18}O$) peaks on the curve of Westerhold et al. (2020).
NSe2 - 13.1 Ma (Major): Occurs in the lower M9 (n12) foram and mid CNM8 nanno Zones, within the Mi-4 cooling event that marks a rapid shift to a higher $\delta^{18}O$ baseline on the curve of Westerhold

et al. (2020).
NSe1 mfs - 13.4 Ma (Medium): Placed midway in. sequence. Placement in middle of a suite of warm peaks (lower $\delta^{18}O$) on the curve of Westerhold et al. (2020) is picked arbitrarily.
NSe1 - 13.8 Ma (Major): Occurs at the base of Serravallian in the upper M7 (N10) foram and CNM7 (NN5) nanno Zones, which also places it in the Mi-3b cooling event at base of the Serravallian Stage. This marks a pronounced shift to a cooler (high $\delta^{18}O$) interval on the curve of Westerhold et al. (2020)

Serravallian (age of the base 13.82 Ma)

NLa1 mfs - 14.9 Ma (Minor): Arbitrarily placed within the Mid-Miocene Climatic Optimum. This interval is a series of five ca. 100-kyr cycles of semi-equal amplitude followed by higher frequency oscillations on the curve of Westerhold et al. (2020).
NLa1 - 15.4 Ma (Minor): Placed in the Mi-2a cooling event in late M5/N8 foram Zone. Dashed because it is suggested by oxygen-isotopic data and not verified in the field - placement is based on the highest values (coolest) on the $\delta^{18}O$ curve of Westerhold et al. (2020).

Langhian (age of the base 15.99 Ma)

NBu4 mfs - 15.99 Ma (Major): The event straddles the Burdigalian-Langhian stage boundary and marks a distinctive warm peak (low $\delta^{18}O$) on the Westerhold et al. (2020) curve.
NBu4 - 16.4 Ma (Major): Placed just above the base of M5 (N8 foram and upper CNM6 nanno Zones and with the M2 cooling event in latest Burdigalian.
NBu3 mfs - 16.9 Ma (Major): Near base of the pronounced warm (low $\delta^{18}O$) interval on Westerhold et al. (2020) curve that extends through the entire late half of this sequence.
NBu3 - 17.4 Ma (Major): Occurs in the early M4/N7 foram and just above the base of CNM6 nanno Zones. Coincides with the onset of Mi-1b cooling event.
NBur2 mfs - 18.0 Ma (Medium): Placed in the middle of sequence. No distinctive warm (lower $\delta^{18}O$) interval within this sequence on the curve of Westerhold et al. (2020) .
NBur2 - 18.5 Ma (Medium): Placed near the middle of M3 foram and NN3 (lower CNM5) nanno Zones. Occurs in the Mi-1ab cooling event. Fine-tuned placement at onset of higher $\delta^{18}O$ (coolest) peaks on the Westerhold et al. (2020) curve.
NBu1 mfs- 18.8 Ma (Medium): Occurs in the M3 foram and CNM5 nanno Zones. Fine-tuned placement is at the onset of warmer (lower O$\delta^{18}O$) interval on the Westerhold et al. (2020) curve.
NBu1 - 19.5 Ma (Medium): Positioned in the uppermost M2 (mid N5) foram and upper CNM4 nanno Zones. This is also the onset of Mi-1aa cooling event and a distinct interval of higher $\delta^{18}O$ on curve of Westerhold et al. (2020).

Burdigalian (age of the base 20.45 Ma)

NAq3 mfs - 19.8 Ma (Medium): The youngest Aquitanian (NAq3) sequence extends into the Burdigalian and the mfs ascribed to this event (NAq3 mfs) thus occurs within the earliest Burdigalian. Placed at onset of several warm peaks (lower $\delta^{18}O$) on the curve of Westerhold et al. (2020).
NAq3 - 20.7 Ma (Major): Occurs just above the base of M1 (N5) foram and CNM4 nanno Zones. It is within Mi-1aa cooling event; which is relatively non-distinctive higher $\delta^{18}O$ interval on the Westerhold et al. (2020) curve.
NAq2 mfs - 20.9 Ma (Minor): Positioned at the base of CNM4 nanno Zone, and earliest part of M2 foram Zone. Marks the onset of warm (lower $\delta^{18}O$) interval on the curve of Westerhold et al. (2020).

NAq2 - 21.5 Ma (Minor): Occurs in the middle of CNM3 nanno and upper M1 foram Zones. Placed at onset of the earliest cool episode (higher $\delta^{18}O$) of the late Aquitanian in the curve of Westerhold et al. (2020).
NAq1 mfs - 22.1 Ma (Major): Placed in the middle of sequence, in mid-M1 foram and near the base of CNM3 nanno Zones. Fine tuned to coincide with a warm peak (low $\delta^{18}O$) in curve of Westerhold et al. (2020).
NAq1 - 23.03 Ma (Major): Occurs near the base of CNM1/NN1 nanno Zone, just above the Stage boundary. Marks the onset of Mi-1 cooling event that starts just before base of Neogene.

Aquitanian (age of the base 23.04 Ma)

PCh2 mfs - 23.8 Ma (Minor): Placed near the middle of sequence. Fine-tuned to be at onset of the warmest (lowest $\delta^{18}O$) peaks in the curve of Westerhold et al. (2020).
PCh2 - 24.8 Ma (Medium): Occurs in the lower O7 foram and mid-NP25 nanno Zones, which coincide with the Oi-2d cooling event.
PCh1 mfs - 25.5 Ma (Minor): Placed in the upper O8 foram and mid-NP25 nanno Zones. No significant isotopic signature, but tuned to the subtle shift from cooler to warmer (lower average $O\delta^{18}O$) on the curve of Westerhold et al. (2020).
PCh1 - 27.1 Ma (Major): Placed near the top of P21 (within O5) foram and at the base of NP24 nanno Zones. Coincides with the base of Oi-2b cooling episode.

Chattian (age of the base 27.29 Ma)

PRu4 mfs - 27.4 Ma (Major): Near end of Rupelian. Fine-tuned to the onset of warm peak (lower $O\delta^{18}O$) on Westerhold et al. (2020) curve in upper-middle part of sequence.
PRu4 - 27.9 Ma (Major): Placed at mid O4 (upper P21) foram Zone, coinciding with the onset of Oi-2a cooling in latest Rupelian, which is a set of $\delta^{18}O$ relative-enrichment peaks in Westerhold et al. (2020) curve. [Note: Base of ratified Chattian Stage is not a SB. The ratified GSSP is younger by ~ 0.5 Myr than the major Oi-2a cooling event].
PRu3 mfs - 28.6 Ma (Major): Placed at the mid-sequence; fine-tuned to be at onset of a relatively warm event (low $\delta^{18}O$) on Westerhold et al. (2020) curve.
PRu3 - 29.3 Ma (Major): Occurs in the upper part of O3/P20 foram Zones. Placed within the Oi-2* cool event after a pronounced warm (low $\delta^{18}O$) episode on Westerhold et al. (2020) curve..
PRu2 mfs - 30.0 Ma (Major): Placed in the upper part of the sequence, at the CNO3/CNO4 nanno zonal boundary where there is a (minor) shift to warmer (lower $\delta^{18}O$) on Westerhold et al. (2020) curve just before "Oi-2" event.
PRu2 - 31.7 Ma (Major): Occurs in the early O2/P19 foram and CNO3 nanno Zones, within the Oi-1b cool interval, fine-tuned to onset of a minor cool (higher $\delta^{18}O$) peak, which is not distinctive.
PRu1 mfs - 32.3 Ma (Medium): Placement uncertain within mid-CNO2 (mid NP22) nanno Zone. Placed here after the Oi-1a cool interval at onset of a slightly warmer (lower $O\delta^{18}O$) interval on the Westerhold et al. (2020) curve in the later part of the sequence.
PRu1 33.8 (Major): Occurs just above the base of Oligocene lower O1 foram and mid NP21 (upper CNE21) nanno Zones. Marks a (major) cooling event (Oi-1) in the $\delta^{18}O$ data of Westerhold et al. (2020).

Rupelian (age of the base 33.9 Ma)

PPr3 mfs - 34.4 Ma (Minor): Placed at CNE21/CNE20 (NP21/NP20) nanno zonal boundary, within a relatively warmer interval prior to the cooling trend in the later part of this sequence.

PPr3 - 35.1 Ma (Minor): Placed at mid-E15 foram and early CNE20 nanno Zones; but due to lack of $\delta^{18}O$ criteria the precise assignment is uncertain.
PPr2 mfs - 35.7 Ma (Minor): Placed near the middle of the sequence; but O$\delta^{18}O$ data are sparse in this interval of the Westerhold et al curve, therefore provisionally placed at possible relatively warmer interval prior to cooling in the later part of the sequence.
PPr2 - 36.7 Ma (Minor): Placed at mid-E14 foram and near the base of NP19 nanno Zones. Coincides with the onset of cooling trend on Westerhold et al. (2020) curve.
PPr1 mfs - 37.2 Ma (Medium): Assigned to the middle of the sequence, but also near onset of the warmest (lowest $\delta^{18}O$) interval on the Westerhold et al. (2020) curve within this sequence.
PPr1 - 37.7 Ma (Major): Occurs at the base Priabonian (GTS20 Paleocene working definition) in the lower P15 (above the base of E14) foram and above the base CNE17 nanno Zones. Within a broad relatively cooler (higher $\delta^{18}O$) interval on curve of Westerhold et al. (2020).

Priabonian (age of the base 37.71 Ma)

PBa1 mfs - 38.0 Ma (Minor): Occurs at E14/E13 foram zonal boundary. No discernable signature seen on the $\delta^{18}O$ curve.
PBa1 - 39.0 Ma (Medium): Placed at mid-E13 foram (mid-CNE15 nanno) Zone. Coincides with a shift to cooler (higher $\delta^{18}O$) interval on Westerhold et al. (2020) curve.

Bartonian (age of the base 41.03 Ma)

PLu4 mfs - 40.4 Ma (Medium): Placed at the E12/E11 (P13/P12) foram zonal boundary. Onset of a pronounced warm interval (lower $\delta^{18}O$) on the curve of Westerhold et al. (2020).
PLu4 - 41.5 Ma (Medium): Placed in the lower E11 (mid P12) foram Zone. Refined to coincide with the onset of a cooling trend in $\delta^{18}O$ on curve of Westerhold et al. (2020).
PLu3 mfs - 42.2 Ma (Minor): Occurs in the late E10 or late-middle CNE13 nanno Zone, but exact calibration is uncertain. Near onset of a slight warming trend after the general cooling trend (increasing $\delta^{18}O$) that dominates the early part of sequence on the curve of Westerhold et al. (2020).
PLu3 - 43.5 Ma (Minor): Occurs at mid-P11 foram zone. Fine-tuned to be at onset of a high amplitude peak (cooling) in $\delta^{18}O$ on the curve of Westerhold et al. (2020).
PLu2 mfs - 44.5 Ma (Medium): Occurs near CNE11/CNE10 nanno zonal boundary. Placed at the onset of a minor warming trend of ~1 Myr on the $\delta^{18}O$ curve of Westerhold et al. (2020).
PLu2 - 46.1 Ma :(Medium): Placed at the CNE10/CNE9 zonal boundary on GTS2020 time scale; but potentially this might be at 46.25 Ma to coincide with onset of cooling interval on the $\delta^{18}O$ curve of Westerhold et al. (2020).
PLu1 mfs - 47.0 Ma (Medium): Placed at mid sequence pending better calibration to isotopic or other records.
PLu1 - 47.8 Ma (Minor):Occurs near the CNE8/CNE7 nanno zonal boundary. Coincides with beginning of relatively cool interval on the $\delta^{18}O$ curve of Westerhold et al. (2020).

Lutetian (age of the base 48.07 Ma)

PYp8 mfs - 48.15 Ma (Major): It coincides with base of the Lutetian Stage at the GSSP section. Fine-tuned to be at beginning of a relative warm interval (low $\delta^{18}O$) on the curve of Westerhold et al. (2020), a trend that continues across Ypresian-Lutetian boundary.
PYp8 - 50.0 Ma (Major): This is a major canyon cutting event in mid-CNE5 (mid-NP13) nanno Zone. Precise age assignment is uncertain - placed here at onset of relatively cooler (higher $\delta^{18}o$) interval on the curve of Westerhold et al, where the main cooling trend begins at ~49 Ma.

PYp7 mfs - 50.2 Ma (Minor): Uncertain age assignment. Placed here at the onset of a (minor) warming ($\delta^{18}O$) trend on curve of Westerhold et al. (2020).
PYp7 - 50.8 Ma (Minor): Occurs at E6/E5 (P8/P7) foram zonal boundary. Placed within a cooling trend on the $\delta^{18}O$ curve of Westerhold et al. (2020).
PYp6 mfs - 50.9 Ma (Minor): Occurs in the upper E5 (P7) foram Zone. Fine-tuned to be at the onset of a sharp cold ($\delta^{18}O$) event on curve of Westerhold et al. (2020).
PYp6 - 51.15 Ma (Minor): Placed within the late E5 (P7) foram Zone. Fine-tuned to be at onset of cool interval ($\delta^{18}O$) on curve of the Westerhold et al. (2020).
PYp5 mfs - 51.4 Ma (Minor): Placed at mid-sequence - fine tuned to be near a warm peak (low $\delta^{18}O$) on the curve of Westerhold et al. (2020).
PYp5 - 51.55 Ma (Minor): Placed at mid E5 (mid P7) foram Zone. Fine-tuned to coincide with onset of a slight cooling trend on the Westerhold et al. (2020) curve.
PYp4 mfs - 52.0 Ma (Minor): Placed at the onset of a warm interval on the $\delta^{18}O$ curve of Westerhold et al. (2020).
PYp4 - 52.4 Ma (Medium): Placed near the E5/E4 (P7/P6b) foram zonal boundary. Also an onset of a cool interval on curve of Westerhold et al. (2020).
PYp3 mfs - 52.8 Ma (Minor): Uncertain age assignment (the assignment here is near the coolest (lowest $\delta^{18}O$) peaks in this sequence in the curve of Westerhold et al. (2020).
PYp3 - 53.6 Ma (Minor): Placed at mid NP11 nanno Zone, but cannot be refined further within a cool dominated (higher $\delta^{18}O$) interval in the curve of Westerhold et al. (2020).
PYp2 mfs - 53.9 Ma (Minor): The age assignment is uncertain (the assignment here seems to be close to a cooling peak in the curve of Westerhold et al. (2020).
PYp2 - 54.2 Ma (Minor): Placed in the lower P6b foram Zone and near base CNE3 nanno Zone, within a high-frequency high-amplitude oscillation in the $\delta^{18}O$ curve of Westerhold et al. (2020)
PYp1 mfs - 55.1 Ma (Minor): Placed near the E2-E3 foram zonal boundary. No signature on $\delta^{18}O$ curve of Westerhold et al. (2020) (This event may need finer tuning).
PYp1 - 55.6 Ma (Medium): Placed within the E2 foram and near at base of CNE2 nanno Zones. No signature is discernable on the $\delta^{18}O$ curve of Westerhold et al. (2020).

Ypresian (age of the base 56.0 Ma)

PTh5 mfs - 56.1 Ma (Minor): Just above PaTh5 SB. Placed at the onset of relatively warmer interval just prior to the PETM excursions in $\delta^{18}O$ discernable.
PTh5 - 56.2 Ma (Minor): Placed in the upper CNP11/NP9 nanno Zones. PaTh5 event has been dated (Sluijs et al., 2008) at less than 200 kyr before the PETM (Hooker, 2015). Coincides with peak in $\delta^{18}O$ (cold interval) on Westerhold et al. (2020) curve.
PTh4 mfs - 56.85 Ma (Minor): Placed near lower P5 foram Zone. Fine-tuned to onset of the warmest interval within this sequence (low $\delta^{18}O$) on the Westerhold et al. (2020) curve.
PTh4 - 57.1 Ma (Medium): Placed at the boundary of P4-P5 foram Zones on GTS2020 time scale. Fine tuned to coincide with onset of a peak in cooling (higher $\delta^{18}O$) in the Westerhold et al. (2020) curve.
PTh3 mfs - 57.35 Ma (Minor): Placed near CNP8 and CNP9 nanno Zonal boundary in the GTS2020 time scale. Fine-tuned to the onset of a relatively warm interval within the sequence as implied by the $\delta^{18}O$ curve of Westerhold et al. (2020).
PTh3 - 57.8 Ma (Minor): Placed at mid-CNP10 nanno Zone. Coincides with a small peak (cooling) in the $\delta^{18}O$ in Westerhold et al. (2020) curve.
PTh2 mfs – 58.0 Ma (Minor): Placed at mid-Sequence - coincides with the sharp onset of a brief warm episode within the sequence according to the $\delta^{18}O$ trends.
PTh2 - 58.2 Ma (Minor): Placed at the base of CNP10 nanno Zone. Placed at the relative cooling

event implied by the $\delta^{18}O$ curve of Westerhold et al. (2020).
PTh1 mfs - 58.5 Ma (Medium): Placed at onset of a warm peak within the sequence according to the $\delta^{18}O$ trends of Westerhold et al. (2020).
PTh1 – 59.0 Ma (Medium): Placed near the boundary of CP8 and CP9 nanno Zones. No significant signature in the $\delta^{18}O$ curve of Westerhold et al, (2020) is discernable

Thanetian (age of the base 59.24 Ma)

PSe2 mfs - 59.9 Ma (Major): Placed at mid-Sequence. No signature discernable in the $\delta^{18}O$ curve.
PSe2 - 60.8 Ma (Major): A prominent canyon-cutting event, placed in the upper CNP7 nanno Zone, lower P4 foram Zone. Fine-tuned to be at onset of (minor) cooling implied in the $\delta^{18}O$ curve of Westerhold et al. (2020), but this shift is quite minor when compared to a major sea-level fall at this event.
PSe1 mfs - 61.0 Ma (Minor): Placed at mid-Sequence. No signature discernable in the $\delta^{18}O$ curve.
PSe1 61.2 Ma (Medium): Placed near the base of NP5 nanno Zone. Fine-tuned at the onset of cooling implied by $\delta^{18}O$ curve of Westerhold et al. (2020) after a warm interval.

Selandian (age of the base 61.66 Ma)

PDa4 mfs - 61.6 Ma (Minor): Placed just above the base of Selandian; although $\delta^{18}O$ curve suggests that the onset of the main warming was at ca. 61.4 Ma.
PDa4 - 61.8 Ma (Medium): Placed within the CNP8 nanno Zone, just before the base of Selandian (a SB by definition); which is 33 precession cycles above base of Chron C26r. "The most prominent of these discontinuities, which marks the base of the[PSe1] sequence, is linked to a long-lasting period of low sea level in the Pyrenees that triggered large erosional collapses along the upper Danian margin and promoted a deep karstification of the Danian platform carbonates ... The basal Selandian represents the correlative conformity of this major discontinuity" (excerpt from Selandian GSSP documentation GTS 2020).
PDa3 mfs - 62.6 Ma (Minor): Placed close to the mid-Sequence and fine tuned to the onset of a warmer interval that dominates upper Da3
PDa3 - 63.5 Ma (Minor): Placed near the lower-middle CP4 nanno Zone. Fine-adjusted to the onset of a (minor) $\delta^{18}O$ cooling event on the Westerhold et al. (2020) curve
PDa2 mfs - 64.1 Ma (Minor): Placed at mid-Sequence (mid PI foram mid CNP3 nanno Zones). Occurs within a relatively warmer interval in the middle of the sequence.
PDa2 - 64.8 Ma (Minor): Placed at upper NP2 (lower CNP3) nanno Zone. Marks the end of a general warming trend through the early Danian.
PDa1 mfs - 65.3 Ma (Minor): In the absence of other criteria, placed at mid-Sequence and within the general warming trend in the $\delta^{18}O$ curve of Westerhold et al. (2020).
PDa1 - 65.8 Ma (Minor): Placed at mid Pa foram Zone. No obvious $\delta^{18}O$ event discernable.

Danian (age of the base 66.0 Ma)

KMa5 mfs - 66.4 Ma (Minor): Same as in Haq, 2014 – placed in the upper *P. hariaensis* foram Zone; coincides with the onset of decrease in $\delta^{18}O$ (implied warming) on the Westerhold et al. (2020) curve that peaks at 66.25 Ma (just before K cooling on their scale).
KMa5 - 66.85 Ma (Minor): Same as in Haq, 2014 – placed at mid *P. hariaensis* foram Zone
KMa4 mfs - 67.8 Ma (Minor): Same as in Haq, 2014; placed at mid-Sequence.
K**Ma4 - 68.75 Ma** (Minor): Same as in Haq, 2014 - migrated to GTS2020 foram zone calibrations (near the base *P. mayarensis* Zone).

5. References cited in section 4.2 (above)

Boulila, S., 2019. Coupling between Grand cycles and events in Earth's climate during the past 115 million years. Sci. Rep. 9, 327. h[ps://doi.org/10.1038/s41598-018-36509-7.

Cramer, B.S., Toggweiler, J.R., Wright, J.D., Katz, M.E. and Miller, K.G., 2009. Ocean overturning since the Late Cretaceous: Inferences from a new benthic foraminiferal isotope compilation. Paleoceanography, v. 24(4).

Dawber, C.F. and Tripati, A.K., 2011. Constraints on glaciation in the middle Eocene (46–37 Ma) from Ocean Drilling Program, Site 1209 in the tropical Pacific Ocean. Paleoceanography, v. 26(2).

Dowsett, H.J. and Cronin, T.M., 1990. High eustatic sea level during the middle Pliocene: Evidence from the southeastern US Atlantic Coastal Plain. Geology, v. 18(5), 435-438.

GTS, 2020. Gradstein F., Ogg, J.G., Schmitz, M.D. and Ogg, G.M. (Eds.), 2020. Geological time scale 2020 , v. 2, Elsevier Science Publishers, Amsterdam.

Gibbard, P.L. and Head, M.J. 2020. The Quaternary Period. In Gradstein F.M. et al. (eds.) The Geological Time Scale 2020. v. 2, 1217-1255.

Haq. B.U., 2014. Cretaceous eustasy revisited. Global and Planetary change, v. 113, 44-58.

Haq, B.U., 2018a. Jurassic sea-level variations: a reappraisal. GSA today, v. 28(1), 4-10.

Haq, B.U., 2018b. Triassic eustatic variations reexamined. GSA Today, v. 28(12), pp.4-9.

Haq, B. U., Hardenbol, J., & Vail, P. R., 1987. Chronology of fluctuating sea levels since the Triassic. Science, v. 235 (4793), 1156-1167.

Haq, B. U., Hardenbol, J., & Vail, P. R., 1988. Mesozoic and Cenozoic chronostratigraphy and cycles of sea-level change. Society of Economic Paleontologists and Mineralogists, v. 42, 71–108.

Hardenbol, J., Thierry, J., Farley, et al, 1998. Mesozoic and Cenozoic sequence chronostratigraphic framework of European basins. In de Graciansky, P.-C., et al. (Eds.), Mesozoic and Cenozoic Sequence Stratigraphy of European Basins. SEPM Special Publication, v. 60, 3-13.

Hearty, P.J., Kindler, P., Cheng, H. and Edwards, R.L., 1999. A +20 m middle Pleistocene sea-level highstand (Bermuda and the Bahamas) due to partial collapse of Antarctic ice. Geology, v. 27(4), 375-378.

Hooker, J.J., 2015. A two-phase mammalian dispersal event across the Paleocene–Eocene transition. Newsletters on Stratigraphy, pp.201-220.

Horita, J., Zimmermann, H. and Holland, H.D., 2002. Chemical evolution of seawater during the Phanerozoic: Implications from the record of marine evaporites. Geochimica et Cosmochimica Acta, v. 66(21), 3733-3756.

Jaffrés, J. B., Shields, G. A., and Wallmann, K. 2007. The oxygen isotope evolution of seawater: A critical review of a long-standing controversy and an improved geological water cycle model for the past 3.4 billion years. Earth Science Reviews, v. 83:83–122

Kaufman, D.S. and Brigham-Grette, J., 1993. Amino-stratigraphic correlations and paleotemperature implications, Pliocene-Pleistocene high-sea-level deposits, northwestern Alaska. Quaternary Science Reviews, v. 12(1), 21-33.

Killingley, J.S., Johnson, R.F. and Berger, W.H., 1981. Oxygen and carbon isotopes of individual shells of planktonic foraminifera from Ontong-Java Plateau, equatorial Pacific. Palaeogeography, Palaeoclimatology, Palaeoecology, v. 33, 193-204

Kocken, I. J., Cramwinckel, M. J., Zeebe, R. E., Middelburg, J. J., and Sluijs, A., 2019. The 405 kyrand 2.4 Myr eccentricity components in Cenozoic carbon isotope records. Clim. Past., doi.org/10.5194/cp-2018-42.

Lea, D., Martin, P.M., Pak, D.K., and Spero, H.I., 2002. Reconstructing a 350 Ky history of sea level using planktonic Mg/Ca and oxygen isotope records from a Cocos Ridge core. Quaternary Science Reviews, v. 21, 283–293.

Lear, C.H., Bailey, T.R., Pearson, P.N., Coxall, H.K. and Rosenthal, Y., 2008. Cooling and ice growth across the Eocene-Oligocene transition. Geology, v. 36(3), 251-254.

Liebrand, D. et al., 2016. Cyclostragraphy and eccentricity tuning of the early Oligocene through earlyMiocene (30.1–17.1Ma): *Cibicides mundulus* stable oxygen and carbon isotope records from Walvis Ridge Site 12. Earth Planet. Sci. Let. 450, 392–405.

Matthews, R.K., 1984. Oxygen-isotopic record of ice-volume history: 100 million years of glacioeustatic fluctuations. AAPG Memoir, v. 36, 97–107.

Matthews, R.K., Poore, R.Z., 1980. Tertiary $\delta^{18}O$ record and glacio-eustatic sea-level fluctuations. Geology v. 8, 501–504.

Miller, K.G., Mountain, G.S., Browning, J.V., et al., 1998. Cenozoic global sea level, sequences, and the New Jersey Transect: results from coastal plain and slope drilling. Reviews of Geophysics, v. 36(4), 3569–601.
Miller, K.G., Kominz, M.A., Browning, J.V., et al., 2005. The Phanerozoic record of global sea-level change. Science, v. 312, 1293–1298.
Miller, K.G., Browning, J.V., Schmelz, W.J., Kopp, et al,, 2020. Cenozoic sea level and cryospheric evolution from deep-sea geochemical and continental margin records. Science Advances., v. 6(20), 1346.
Olson, S.L. and Hearty, P.J., 2009. A sustained+ 21 m sea-level highstand during MIS 11 (400 ka): direct fossil and sedimentary evidence from Bermuda. Quaternary Science Reviews, v. 28(3-4), 271-285.
Pälike, H., Norris, R.D., Herrle, J.O., Wilson, P.A., Coxall, H.K., Lear, C.H., Shackleton, N. J., Tripa=,A.K., Wade, B.S., 2006. The Heartbeat of the Oligocene climate System. Science 314,1894–1898.
Pearson, P.N., 2012. Oxygen isotopes in foraminifera: Overview and historical review. The Paleontological Society Papers, v. 18, 1-38..
Raymo, M.E., Mitrovica, J.X., O'Leary, M.J., DeConto, R.M. and Hearty, P.J., 2011. Departures from eustasy in Pliocene sea-level records. Nature Geoscience, v. 4(5), 328-332.
Raymo, M.E. and Mitrovica, J.X., 2012. Collapse of polar ice sheets during the stage 11 interglacial. Nature, v. 483(7390), 453-456.
Rosenthal, Y., Boyle, E.A. and Slowey, N., 1997. Temperature control on the incorporation of magnesium, strontium, fluorine, and cadmium into benthic foraminiferal shells from Little Bahamas Bank: Prospects for thermocline paleoceanography. Geochimica et Cosmochimica Acta, v. 61(17), 3633-3643.
Sluijs, A., Brinkhuis, H., Crouch, E.M., John, C.M., Handley, L., Munsterman, D., Bohaty, S.M., Zachos, J.C., Reichart, G.J., Schouten, S. and Pancost, R.D., 2008. Eustatic variations during the Paleocene-Eocene greenhouse world. Paleoceanography, v. 23(4), 18 pp.
Stanley, S.M. and Hardie, L.A., 1998. Secular oscillations in the carbonate mineralogy of reef-building and sediment-producing organisms driven by tectonically forced shifts in seawater chemistry. Palaeogeography, Palaeoclimatology, Palaeoecology, v. 144(1-2), 3-19.
Vail, P.R., Mitchum Jr, R.M. and Thompson III, S., 1977. Seismic stratigraphy and global changes of sea level: Part 4. Global cycles of relative changes of sea level.:. AAPG Memoir 26, p. 63.
Veizer, J., Ala, D., Azmy, K., Bruckschen, P., et al., 1999. 87Sr/86Sr, δ13C and δ18O evolution of Phanerozoic seawater. Chemical geology, v. 161(1-3), 59-88
Veizer, J. and Prokoph, A., 2015. Temperatures and oxygen isotopic composition of Phanerozoic oceans. Eart Science Reviews v. 146, 92-104.
Wade, B.S., Pälike, H., 2004. Oligocene climate dynamics. Paleoceanography 19, PA4019. doi:10.1029/2004PA001042.
Westerhold, T., Marwan, N., Drury, A.J., et al., 2020. An astronomically dated record of Earth's climate and its predictability over the last 66 million years. Science, v. 369(6509), 1383-1387.
Wilkinson, B.H. and Algeo, T.J., 1989. Sedimentary carbonate record of calcium-magnesium cycling. American Journal of Science, v. 289(10), 1158-1194.
Zachos, J., Pagani, M., Sloan, L., Thomas, E., and Billups, K., 2001. Trends, rhythms, and aberrations in global climate 65 Ma to Present. Science, v. 292, 686-693.
Hooker, J.J., 2015. A two-phase mammalian dispersal event across the Paleocene–Eocene transition. Newsletters on Stratigraphy, pp.201-220.

6. Global documentation of sequence boundaries

In our original Meso-Cenozoic synthesis of sea-level variations (Haq et al., 1988) we made a special effort to incorporate sequence-stratigraphic data from the stratotype sections of the Standard Stages (located mostly in northwestern and southern Europe). Ascertaining the sequence-stratigraphic positioning of the sea-level highs and lows within these chronostratigraphic units that had been designated as the global standard by the geological community was deemed necessary for achieving greater chronologic coherence, especially if the widely-distributed synchronous sea-level fall events (represented by erosional surfaces of variable severity) were to be placed in a proper global context. Much of the early documentation for the third-order Meso-Cenozoic sequences came from the offshore subsurface seismic sections (with limited well-ties) that were recorded in various parts of the world, albeit with less age control (e.g., Vail et al., 1977). In the 1987-88 reconstruction

of the Mesozoic and Cenozoic cycle charts we added on-land well log and outcrop studies with greater chronologic control, and the latter was accomplished entirely from the public domain sections where our conclusions could be independently tested (Haq et al., 1988). This testing of the original eustatic framework has gone on for over three decades and its basic tenet has been repeated confirmed. There was an important update of Haq et al. (1988) framework in which the European basins were reconsidered in greater detail (Hardenbol et al., 1998) and a number of additional sequence cycles were added to the Cenozoic (45 vs 53, several of the latter were fourth-order cycles not identified earlier in sediment input areas). Both of those syntheses form the basis of the current update.

In the five years preceding the 1987-88 publications outcrop studies in search of Stage stratotypes were conducted in northwestern and southern Europe, including what were considered to be the stratotype (or neo-stratotype) sections of the Standard Stages at that time (in addition to studies in North America, Australia, New Zealand and elsewhere). Nevertheless, many of the originally designated Stage stratotypes had either been obscured (e.g., by urban development) or completely destroyed (e.g., quarries that had been fully exploited for their content and then leveled and/or covered up). A good example was the stratotype of the Chattian Stage in northern Germany, where in 1968 the "friends of the Chattian" (as we designated ourselves) were able to study the outcrop and collect the last samples from the quarry before the waiting bulldozers stepped in even before we had left the quarry to level the landscape for a new development. In such cases new reference sections (neo-stratotypes) had to be found (see GTS 2020 for the current Stage reference sections).

For our earlier synthesis (Haq et al., 1987, 1988) the Cenozoic depositional sequences were documented from southern England and northwestern Europe (Belgium, France, Germany) and southern Europe (Italy and Spain), the US Gulf Coast, North Carolina, as well as New Zealand and Australia. Since those studies, together with the update of Hardenbol et al., 1998, form the basis of this revision, and also for completeness, we summarize those locations here (from Haq et al., 1988): On the Isle of Wight a relatively complete late Paleocene to early Oligocene section is exposed at White Cliff and Alum Bays with most of sequences identified in earlier syntheses and here. Also documented from southern England sections in Herne Bay (Thanetian stratotype), Barton (Bartonian stratotype) and on Sheppy Island (Ypresian) that are key to the construction of the mid Paleocene and early Eocene framework. In Belgium the localities included the type areas of Rupelian Stage at Sint Niklaas, Kruibeke and Steendorp and sections in Pellenberg and Tongeren (stratotype for Tongrian Stage = Latdorfian, earliest Rupelian). In the type area of Ypresian Stage the documentation came from sections at the Kortemark, Egem and Aalbeke localities; the sections at Balegem (type Ledian = middle Lutetian), at Wemmel (type Wemmalian = late Lutetian), the Ciply section in Mons Basin (type Montian = ~ Selandian), at Zetrud-Lumay and Briane l'Alleud (type Bruxellian = early Lutetian), Gelinden (Thanetian), and Vroenhoven along the Albert Canal (for the Cretaceous-Paleocene transition).

In France, Paris Basin was a key region, where the documentation came from numerous localities. Near the villages of St. Leu d'Esserent and St. Vaast-les-Melo the type area of the Lutetian Stage and other sections of the same age at Guitrancourt and Damery shed light on the mid Eocene. The stratotype of the regional Stage Cuisian (= late Ypresian) was studied at Cuise-la-Motte and Gisors. Other sections in Paris Basin included the outcrops of local Stages: at Auvers-sur-Oise (type section for Auversian = ~Bartonian), at Marine (type Marinesian = late Bartonian), at Pourcy (type Sparnacian = early Ypresian), at Cormeilles (type area for Stages: Stampian = ~Rupelian; Sannoisian = middle Rupelian; and Ludian = ~Priabonian) and at Chalons-sur-Vesle (Thanetian). In southern France sections included outcrops in the type area of Aquitanian Stage at Moulin de Bernachon, Moulin de l''Eglise and L'Ariey, as well as a section at Grignols that spans the late Aquitanian to early Burdigalian interval. The type area for the Burdigalian Stage included the sections studied at Champ du Peloua, Ruisseu de la Coquilleyre, and Pont Pourquey, La Sime. Elsewhere in NW Europe, studied

sections included the stratotype of Chattian Stage at Doberg bei Bünde, in northern Germany (Haq et al., 1988).

In southern Europe, sections included the type area for regional Stage Ilerdian (= early Ypresian) at Tremp, Lerida in northern Spain; and stratotype of Priabonian Stage at Priabona in northern Italy. (Note: type sections that had been destroyed or where we either had no access or those that had been obscured by urbanization, were nevertheless studied to obtain sequence documentation via the literature where original sections had been measured and described, especially for the Late Neogene in Italy, including sections for type areas of Langhian, Serravallian. Tortonian, Messinian, Zanclean and Calabrian Stages (Haq et al., 1988). All of these formed the basis of our chronostratigraphic framework for the Cenozoic.

In the United States sequence-stratigraphic studies were carried out in sections along the East Coast: In North Carolina, the quarry near Belgrade (early Miocene); the Trent River section (Oligocene); quarry near New Bern (late Eocene-Oligocene); the Ideal Quarry in New Hannover County (middle Eocene); and quarry outcrop at Santee Portland (late Eocene). Along the Gulf of Mexico Coast sections in Alabama included Little Staves Creek (middle Eocene-Oligocene); quarry at St. Stephens (latest Eocene-early Miocene), sections exposed along the Tombigbee and Chattahoochee Rivers (Paleogene); and the Braggs section for the Cretaceous-Paleocene transition (Haq et al., 1988).

On New Zealand's South Island coastal sections provided documentation for much of the Paleogene that included outcrops from South Canterbury to North Otago, which provided documentation for the Eocene to middle Miocene sequences; outcrops at North Canterbury (late Cretaceous to Oligocene); and sections along the west coast, between Greymouth and Karamea (Eocene-middle Miocene). The Australian sections also provided documentation for a nearly complete Paleogene, as well as much of the Neogene. We studied sections along the Otway Mountains that included: along the eastern flanks of the Otways, outcrops at Bells Headland, Airey's Inlet and Soapy Rocks (latest Eocene to early Miocene); at the southwest end of the Otways, the section at Browns Creek (late Eocene-early Oligocene); along the western flanks of the Otways, sections at Pebbles Point (middle Paleocene-Oligocene) and Port Campbell (early Miocene-Pliocene) (Haq et al., 1988).

Further documentation for the Cenozoic sequence cycles is extensive and has accumulated over the last three and half decades from around the world. We have widely perused the published works for such information and where biostratigraphy and/or isotopic stratigraphy allows, placed the local and regional findings within the global framework. At many localities because of the influence of local tectonics, the stratigraphy shows little or no correlation to the global mean eustatic curves presented here. But there are many areas that do match up and those are listed individually for each depositional cycle in the following sections. However, even when an area correlates well with the overall trends, one should not expect to find every event listed on the eustatic charts in any particular segment of time, or the amplitudes of rise and fall values to be entirely similar to the global average, As discussed in the main text this is translated locally by the depositional system on how and when local tectonics (subsidence rates) and sediment supply rates either enhance or subdue the underlying eustatic signal, or may even completely overwhelm this signal producing a totally variant stratigraphy. This is why when perusing the sea-fall events (sequence boundaries) as to where they have been documented, you may notice that at any particular locality, not all of the SBs on the global mean list may be represented. This is to be expected also, considering the variable rigor of the analyses and other limitations.

6.1 *Additional (more recent) documentation of sequence cycles*

In addition to the studies carried out globally for the original synthesis of the Cenozoic discussed above (see also, Haq et al., 1988), in the sections below we list the additional documentation for the

individual depositional cycles as identified by their alphanumeric numbers on the Cycle Charts (Figs. 1 and 2, in the main text, and Fig. S1 below). Under each cycle boundary we list the localities and numbered references (appended at the end) in which that particular SB was identified (or has been interpreted/reinterpreted by us as belonging to that cycle).

As stated iearlier, the various Stage type reference sections in Europe and their placement within the global chrono-eustatic framework were covered in our first synthesis of the Cenozoic (Haq et al., 1988, numbered ref. # **1** in the list below) and further elucidated in de Graciansky et al. (1998, # **2,** in the list below) wherein several sections of the Cenozoic in Europe were studied in more detail. Most sequence cycles listed below were first identified and dated in ref. **1**, and some additional cycles were added in the studies reported in ref. **2** (all ages having been updated here *fide* GTS2020). We do not repeat the documentation already reported in Haq et al., 1988 (**1**). However, we include reference to the new studies reported in ref. **2** even when some of these localities already appeared in the first synthesis (see, e.g., ref. # **3, 4, 10, 14, 16** and **23** in the list at the end of this section).

We have made an effort to identify (and where necessary update the positioning and numerical age) of much of the Cenozoic depositional cycles found in the open literature. However, it is apparent that we may have missed some of the documentation reported in literature that was not accessible to us (some publisher's egregiously block accesses to academic literature), or where the age assignment data could not be converted easily to correspond to the modern bio-chronostratigraphic schemes. Thus, the additional documentation section below should be considered a "work in progress" and should continue to grow as more articles and details become accessible.

Danian (age of the base 66.0 Ma). Also the base of Cenozoic, Paleogene and Paleocene.
The Maastrichtian-Danian transition, in spite of being a major catastrophic event in Earth history when asteroidal impact(s) decimated both marine and terrestrial species, is not a major boundary in the sequence-stratigraphic sense. Although impact ejecta deposits are evident near the impact site in the Caribbean, as are tsunami deposits, the Cretaceous-Paleogene (K-P) transition occurred during a relative highstand of sea level. The infection point from the highstand to the low-point in the sea level is placed some 200 Kyr later than the K-P boundary event, and the sea-level drop here is a relatively minor event (<25 m of fall). The first three Danian sea-level falls were minor, the youngest, PDa4, is considered a medium amplitude fall (25-75 m).
PDa1 - 65.8 Ma (Minor): This event occurred shortly after K-P boundary and was a relatively minor sea-level fall. Originally documented from NW Europe, it's later confirmation has come from the basins in Belgium bordering southern North Sea shelf (Vandenberghe et al. 1998 ref. **3**), the Basque Basin in Spain (Pujalte et al., 1998, ref. 4), Bulgaria (Stoykova and Ivanov, 2002, ref. **5**), and from the Sinai Peninsula (Lüning et al., 1998, ref. **6**) and Egypt (Farouk, 2016, ref. **7**). **PDa2 - 64.8 Ma** (Minor): In addition to NW Europe the second minor cycle in the Danian is also documented from Bulgaria (**5**) Sinai (**6**)**,** Egypt (**7**) and the Greater Indus Basin of Pakistan (Afzal et al., 2009, ref. **8**). **PDa3 - 63.5 Ma** (Minor): Documented from Belgium (**3**), the Basque Basin (**4**), Bulgaria (**5**), Sinai (**6**) and a potential occurrence also in the Indus Basin in Pakistan (**8**). **PDa4 - 61.8 Ma** (Medium): This cycle ends in a more prominent sea-level falls than the first three cycles in the Danian. It occurs near the Danian-Selandian transition. In Europe it was documented from NW Europe (**1**) the Faeroe Basin in northern Barents Sea (Mitchell et al., 1993, ref. **9**) and the Basque Basin (**4**), and Bulgaria (**5**), outside Europe it has been recorded in the Sinai (**6)** and Egypt (**7**).

Selandian (age of the base 61.66 Ma)
The Selandian was not as yet designated as formal Stage at the time of our first Cenozoic synthesis (1988, ref **1**), but by the time ref. **2** had been published it was already a formal Stage (carved mostly

out of the older Thanetian). Two prominent sequence boundaries were identified in this Stage in the European basins (ref. **2** and other references therein).
PSe1 61.2. **Ma** (Medium): A medium amplitude sea-level fall (25-75 m), it's most recent documentation comes from Belgium (**3**), the Faeroe Basin (**9**), Eastern North Sea Basin (Michelsen et al., 1998, ref. **10**) and Egypt (**7**). **PSe2 - 60.8 Ma** (Major): This is a major amplitude SB (>75 m) that was originally recorded in NW Europe (ref. **1** where it was included in early Thanetian). It's more recent documentation has come from the Faeroe Basin (**10**), the Basque Basin (**4**), Sinai (**6**), Egypt (**7**) , as well as Southern Australian margin (McGowran et al., 2004, ref. **11**). The Australian basins include South Australian onshore and offshore as well as the Great Australian Bight.

Thanetian (age of the base 59.24 Ma):
PTh1 – 59.0 Ma (Medium): The first sequence cycle of the Thanetian, which ends in a medium amplitude sea-level fall (25-75 m) has been recorded in Belgium bordering the southern North Sea (3), the Faeroe Basin in northern Barents Sea (**9**), Sinai (**6**), Egypt (**7**) and Pakistan (**8**). **PTh2 - 58.2 Ma** (Minor): A minor amplitude event that has been recently further documented from the Faeroe Basin (**9**) and Sinai (**6**). **PTh3 - 57.8 Ma** (Minor): Another minor event that has been confirmed occurring in Belgium (**3**), the Faeroe Basin (**9**), the Basque Basin (**4**) and Sinai (**6**). **PTh4 - 57.1 Ma** (Medium): A prominent fall that has been documented widely form Belgium (**3**), the Faeroe Basin (**9**), the Basque Basin (**4**), Egypt (**7**), Pakistan (**8**), and South Australia (**11**). **PTh5 - 56.2 Ma** (Minor): The youngest of the Thanetian depositional cycle boundary occurs close to the Thanetian-Ypresian transition and has been reported from the Belgium (**3**), Eastern North Sea (**10**), the Faeroe Basin (**9**), Egypt (7) and Pakistan (**8**).

Ypresian (age of the base 56.0 Ma). Also the base of Eocene.
The Ypresian is characterized by several minor and two medium amplitude sea-level fall events, ranging in duration from 0.4 to 1.4 Myr, thus at least one of these was a fourth order cycle. Ypresian is well studied in Belgium and the Paris Basin (1) where originally six cycles were identified to which two were added later (**2**, and references therein).
PYp1 - 55.6 Ma (Medium): Recorded in Belgium bordering southern North Sea shelf (**3**), Eastern North Sea (**10**), the Faeroe Basin (**9**), Sinai (**6**) and Pakistan's Indus Basin (**8**). **PYp2 - 54.2 Ma** (Minor): Recently confirmed to occur in Belgium (**3**). **PYp3 - 53.6 Ma** (Minor): Also confirmed to occur in Belgian shelf section bordering southern North Sea. (**3**). **PYp4 - 52.4 Ma** (Medium): Confirmed to occur in Belgium (**3**), South Australia (**11**) and potentially also in the Indus Basin of Pakistan (**8**). **PYp5 - 51.5 Ma** (Minor): Documented in the Belgium (**3**) and South Australia (**11**). **PYp6 - 51.1 Ma** (Minor): also documented in the Belgium (**3**) and South Australia (**11**). **PYp7 - 50.8 Ma** (Minor): Outside NW Europe this event has been reported from South Australia (**11**). **PYp8 - 50.0 Ma** (Major): The only major sea-level fall (>75 m) of the Ypresian Stage. Outside NW Europe it has a potential occurrence in the Indus Basin of Pakistan (**8**).

Lutetian (age of the base 48.07 Ma)
The Lutetian Stage is also well studied for its sequence-stratigraphic framework (in Paris and other NW European basins). It is characterized by two minor and two medium amplitude sea-level fall events, all of which were originally identified from NW Europe (**1**).
PLu1 - 47.8 Ma (Minor): This event has been confirmed as occurring in both the southern North Sea shelf in Belgium (**3**) and Eastern North Sea (**10**). **PLu2 - 46.1 Ma** (Medium): In addition to the Belgian sections (**3**), the event has been documents from the Faeroe Basin (**9**), the Indus Basin of Pakistan (**8**) and may also potentially occur in New Zealand's offshore Taranaki Basin (Higgs et al., 2012, ref. **12**). **PLu3 - 43.5 Ma** (Minor): Like the previous cycle this event is also reported from Belgium (**3**), the Faeroe Basin (**9**), Pakistan (**8**) and confirmed to occur in the New Zealand's Taranaki Basin (**12**). **PLu4 - 41.5 Ma** (Medium): The youngest of the Lutetian SB is a prominent

one that has also been reported from the same four basins as the previous event (**3**, **8**, **9**, and **12**); in addition it has also been documented from South Australia and the Great Australian Bight (**11**).

Bartonian (age of the base 41.03 Ma)
The Bartonian is also well studied in NW Europe (**1**) where in the mid Stage only a single prominent (medium amplitude) sea-level fall event was recorded. **PBa1 - 39.0 Ma** (Medium): This event has since been confirmed occurring in the Belgium bordering the southern North Sea shelf (**3**), the Faeroe Basin (**9**), South Australian Basin and the Great Aussie Bight (**11**), and in New Zealand's offshore Taranaki Basin (**12**).

Priabonian (age of the base 37.71 Ma):
PPr1 - 37.7 Ma (Major): A major event that has been documented from Belgium (**3**), the New Jersey margin of the US (Miller et al., 1998, ref. **13**), the Great Australian Bight (**11**), New Zealand's offshore Taranaki Basin (**12**) and potentially also from the Faeroe Basin (**9**). **PPr2 - 36.7 Ma** (Minor): Also reported from the first four basin's of the previous cycle (**3**, **11**, **12**, **13**), and has a confirmed occurrence in the Faeroe Basin (**9**), as well as South Australia (**11**). **PPr3 - 35.1 Ma** (Minor): The youngest of the Priabonian cycle is repeated in Belgium, the Faeroe Basin and in New Zealand (**3**, **9**, **12**), South Australia and the Great Australian Bight (**11**), and may potentially also occur in the Indus Basin of Pakistan (**8**).

Rupelian (age of the base 33.9 Ma). Also, the base of Oligocene.
For the Rupelian Stage originally only three third-order depositional cycles were reported from northern Europe (**1**); an additional event was added later (**2**) and all four have now been documented widely. As the Earth was entering icehouse conditions starting at the Eocene-Oligocene transition, all four sea-level falls of the Early Oligocene manifest themselves as major events (>75m), implying large ice sheet development on Antarctica. **PRu1 33.8 Ma** (Major): This event has now been recorded from the Faeroe Basin (**9**), the Eastern North Sea (**10**), the Pannonian Basin of Hungary (Vakacs et al., 1998, ref. **14**), the Zagros Fold-Belt part in Kurdistan (Ameen-Lawa et al., 2015, ref. **15**), New Jersey margin (**13**) and South Australia and the Great Aussie Bight (**11**). **PRu2 - 31.7 Ma** (Major): Documented widely from the Eastern North Sea (**10**), the Pannonian Basin (**14**), the Piedmont Basin of Italy (Gnaccolini et al., 1998, ref. **16**), the Albemarle Basin offshore North Carolina in the US (Coffey and Read, 2007, ref. **17**), and potentially also from the New Jersey margin (**13**). **PRu3 - 29.3 Ma** (Major): Found in the Pannonian Basin (**14**), the New Jersey margin (**13**) and potentially also in Kurdistan (**15**). **PRu4 - 27.9 Ma** (Major): This event is reported widely from the Eastern North Sea (**10**), the Pannonian Basin (**14**), the Piedmont Basin (**16**), from the Great Bahamas Bank's carbonate buildups (Eberli and Ginsburg, 1989, ref. **18**), the New Jersey margin (**13**), offshore North Carolina (**17**) and South Australia (**11**).

Chattian (age of the base 27.29 Ma)
Two prominent third-order depositional cycles were recorded in the Chattian of NW Europe (**1**). Their ages have now been refined (as discussed above). **PCh1 - 27.1 Ma** (Major): Outside NE Europe this event has additionally been documented from the Pannonian Basin (**14**), the Piedmont Basin (**16**), the New Jersey margin (**13**), offshore North Carolina (**15**), South Australia and the Great Australian Bight (**11**), and potentially also from Kurdistan (**15**). **PCh2 - 24.8 Ma** (Medium): This event has been recorded from Belgium (**3**) , the Pannonian Basin (**14**), the New Jersey margin (**13**), and potentially also in Kurdistan (**16**).

Aquitanian (age of the base 23.04 Ma). Also the base of Neogene and Miocene
The Aquitanian has two major sea-level fall events, intervened by a minor one, where the major falls are considered to beassociated with ice-sheet expansion events on Antarctica**. NAq1 - 23.03 Ma**

(Major): A major fall that has been documented from Belgium (**3**), Eastern North Sea (**10**), the Pannonian Basin (**14**), the Piedmont Basin (**16**), the Great Bahamas Bank (**18**), the New Jersey margin (**13**), the North Carolina offshore (**17**), and South Australia and the Great Australian Bight (**11**). **NAq2 - 21.5 Ma** (Minor): This minor fall has been recorded in Eastern North Sea (**10**), the Pannonian Basin (**14**), Kurdistan (**15**), the Great Bahamas Bank (**18**), the New Jersey margin (**13**), the Great Australian Bight (**11**) and potentially also in McMurdo Sound of Antarctica (Bartek et al., 1996, ref. **19**). **NAq3 - 20.7 Ma** (Major): Another prominent sea-level fall in the Aquitanian that is recorded widely, in the Eastern North Sea Basin (**10**), the Pannonian Basin (**14**), the Piedmont Basin (**16**), the Great Bahamas Bank (**18**), the New Jersey margin (**13**) and the Great Australian Bight (**11**).

Burdigalian (age of the base 20.45 Ma)
NBu1 - 19.5 Ma (Medium): Outside southern Europe, the documentation for this event comes from the Pannonian Basin (**14**) and potentially also from the New Jersey margin (**13**). **NBur2 - 18.5 Ma** (Medium): Recorded from Belgium (**3**), the Eastern North Sea Basin (**10**), the Pannonian Basin (**14**), the Piedmont Basin (**16**), the New Jersey margin (**13**) and the Great Australian Bight (**11**). **NBu3 - 17.4 Ma** (Major): Documented in the Eastern North Sea, the Pannonian Basin (**14**), the Piedmont Basin (**16**) and offshore Louisiana, in the US (Hentz and Zeng, 2003, ref. **20**). **NBu4 - 16.4 Ma** (Major): Documented widely from Belgium (**3**), Eastern North Sea Basin (**10**), the Pannonian Basin (**14**), the Great Bahamas Bank (**18**), the New Jersey margin (**13**), the offshore Louisiana (**20**) South Australia (**11**) and McMurdo Sound (**19**).

Langhian (age of the base 15.99 Ma)
A single sequence cycle boundary has been recorded in the Langhian. **NLa1 - 15.4 Ma** (Minor): A relatively minor fall that is, nevertheless, reported widely from the Eastern North Sea Basin (**10**), the southeastern North Sea Basin (Sørensen e al., 1995, ref. **21)**, the Pannonian Basin (**14**), the Piedmont Basin (**16**), the Transylvanian Basin in Romania (Krézsek and Filipescu, 2005, ref. **22**), the Great Bahamas Bank (**18**), the New Jersey margin (**13**), the McMurdo Sound in Antarctica (**19**), and potentially also from offshore Louisiana (**20**).

Serravallian (age of the base 13.82 Ma)
All three Serravallian sea-level fall events were of major amplitude (>75 m) associated with ice sheet expansion. **NSe1 - 13.8 Ma** (Major): This event has been documented from the Pannonian Basin (**14**), the Transylvanian Basin (**22**), Kurdistan (**15**), the Great Bahamas Bank (**18**), the New Jersey margin (**13**) the Louisiana offshore (**20**) and the Great Australian Bight (**11**). **NSe2 - 13.1 Ma** (Major): The second major event of the Serravallian had an even wider record, in addition to the Pannonian, Transylvanian, Kurdistan, Bahamas, New Jersey and offshore Louisiana Basins, it is also documented in the southern North Sea (**21**) and McMurdo Sound (**19**). **NSe3 - 11.7 Ma** (Major): In addition to the sites mention in the previous cycle (southern North Sea, Pannonian, Transylvanian, Kurdistan, Bahamas, New Jersey, Louisiana Basins, and McMurdo Sound) this event also occurs in the Piedmont Basin (**16**) and South Australia Basin and the Great Aussie Bight (**11**).

Tortonian (age of the base 11.62 Ma)
A single prominent SB occurs in the middle of the Tortonian Stage**. NTo1 - 9.3 Ma** (Medium): Outside the type area this event has been documented in Eastern North Sea Basin (**10**), in Transylvanian Basin in Romania (**22**), in the Great Bahamas Bank (**18**), in offshore Louisiana (**20**), in the deltaic sediments of the Foz do Amazonas Basin, Brazil offshore (Gorini et al., 2014, ref. **23**), at the Great Australian Bight (**11**) and in the McMurdo Sound (**19**).

Messinian (age of the base 7.25 Ma)

The Messinian Stage encompasses two depositional cycles, the older starting at almost at the Tortonian-Messinian transition, but within the Messinian. **NMe1 - 7.2 Ma** (Major): It is a major sea-level fall event and outside the type area it has been documented in southeastern North Sea (**21**), the Great Bahamas Bank (**18**), Louisiana offshore (**20**), the Amazon Basin (23), the Great Australian Bight (**11**), and in the McMurdo Sound (**19**). **NMe2 - 5.75 Ma** (Major): The second major SB occurs in the late Messinian, shortly before the end of the Messinian Salinity Crisis in the Mediterranean (5.97 to 5.3 Ma). This event at 5.75 Ma has been recorded from Belgium (**3**), Eastern North Sea (**21**), Louisiana offshore (**20)**, the Great Bahamas Bank (**18**), the Amazon Basin (**23**) and South Australia and the Great Australian Bight (**11**).

Zanclean (age of the base 5.33 Ma)
NZa1 - 4.6 Ma (Major): A major sea-level fall event that has been documented from Belgium **(3**), southeastern North Sea (**21**), central Mediterranean and sections in Italy (Catalano et al., 1998, ref. **24**), the Great Bahamas Bank (**18**), Louisiana offshore (**20**), the Amazon Basin (**23**) and in the McMurdo Sound (**19**), **NZa2 - 4.15 Ma** (Major): The second Zanclean major sea-level fall has been recorded in Belgium (**3**), southeastern North Sea (**21**), central Mediterranean (**24**), the Great Bahamas Bank (**18**), the Amazon Basin (**23**) and the McMurdo Sound (**19**).

Piacenzian (age of the base 3.6 Ma)
NPi1 - 3.3 Ma (Major): A major third-order event documented from Belgium (**3**), Eastern and southeastern North Sea (**10**, **21**), central Mediterranean (**24**), the Great Bahamas Bank (**18**), the Amazon Basin (**23**), South Australia and the Great Aussie Bight (**11**), and the offshore Canterbury Basin in New Zealand (Lu and Fulthorpe, 2004, ref. **25**). **NPi2 - 2.73 Ma** (Major): Also a major sea-level fall recorded in Belgium (**3**), Eastern North Sea (**10**), the mid-Norway margin (Rise et al., 2005, ref. **26**), central Mediterranean (**24**), the Great Bahamas Bank (**18**), the Amazon Basin (**23**) and the offshore Canterbury Basin (**25**).

Gelasian (age of the base 2.58 Ma); Also base of the Quaternary
In the Quaternary all identified sequence boundaries are fourth- or fifth-order and the sea-level falls tend to be of medium to major amplitudes. **QGe1 - 2.54 Ma** (Major): Reported from mid-Norway margin and Barents Sea (Hafeez, 2011, ref. **27**), the Great Bahamas Bank (**18**), the Amazon Basin (**23**), and New Zealand's offshore Canterbury Basin (**25**). **QGe2 - 2.15 Ma** (Medium): Documented in mid-Norway margin and Barents Sea (**17**), where it is also reported from the Bjørnøya Fan (Alexandropoulou, 2013, ref. **28**), and in the Great Australian Bight (**11**).

Calabrian (age of the base 1.8 Ma)
QCa1 - 1.7 Ma (Medium): This event has been documented from mid Norway margin and Barents Sea (**26**, **27**), the Bjørnøya Fan (**28**), the Amazon Basin (**23**), and New Zealand's Canterbury Basin (**25**). **QCa2 - 1.5 Ma** (Medium): Reported from the Barents Sea (**27**) and Bjørnøya Fan (**28**), the Great Bahamas Bank (**18**), the Amazon Basin (**23**), the Great Australia Bight (**11**), and the offshore Canterbury Basin (**25**). **QCa3 - (MIS22) - 0.90 Ma** (Major): Reported from Bjørnøya Fan (**28**), and the Great Bahamas Bank (**18)**, with a possible occurrence also on the mid-Norway margin (**26**).

Chibanian (age of the base 0.77 Ma)
QCh1 - (MIS16) - 0.68 Ma (Major): Reported from Bjørnøya Fan (**28**) and Barents Sea (**27**), and the Amazon Basin (**23**). **QCh2 - (MIS 14) - 0.57 Ma** (Medium). Recorded in the Barents Sea (**27**). **QCh3 - (MIS12) - 0.47 Ma** (Major): Documented from the Bjørnøya Fan (**28**), the Barents Sea (**27**), the mid Norwegian margin (**26**), and the offshore Canterbury Basin of New Zealand (**25**). **QCh4 - (MIS10) - 0.38 Ma** (Major): Recorded in the Barents Sea (**27**). **QCh5 - (MIS8) - 0.28 Ma** (Major):

Reported from the mid-Norwegian margin and Barents Sea (**26**, **27**), and the Canterbury Basin (**25**).
QCh6(MIS6) - 0.18 Ma (Major): Reported from the Barents Sea and the Bjørnøya Fan (**27**).

Late Pleistocene (age of the base 0.129 Ma)
QLGM - 0.033 Ma (Major): The event placed at the inflexion point of the drop in sea level at the initiation of the last glacial maximum is a major sea-level fall along many margins of the world. Our list only shows some of these occurrences, in the Barents Sea, the Bjørnøya Fan and the mid-Norway margin (**27**, **28** and **26**), southeastern North Sea (**21**), the Great Bahamas Bank (**18**) and the offshore Canterbury Basin in New Zealand (**25**).

7. Numbered References for additional documentation section 6.1 (above)

(1) Haq, B. U., Hardenbol, J., & Vail, P. R., 1988. Mesozoic and Cenozoic chronostratigraphy and cycles of sea-level change. SEPM Special Publications, v. 42, p. 71–108.
(2) de Graciansky, P-,C., Hardenbol, J., Thierry, J., Vail, P.R., 1998 (Eds.). Mesozoic and Cenozoic sequence stratigraphy of European Basins. SEPM Special Publication, v. 60, 786 pp.
(3) Vandenberghe, N., Laga, P., Steurbaut, E., Hardenbol, J. and Vail, P.R., 1998. Tertiary Sequence Stratigraphy at the Southern Border of the North Sea Basin in Belgium. SEPM Special Publications, v, 60, p. 119-154.
(4) Pujalte, V., Baceta, J.I., Orue-Etxebarria, X. and Payros, A., 1998. Paleocene Strata of the Basque Country, Western Pyrenees, Northern Spain: Facies and sequence development in a deep-water starved basin. SEPM Special Publications, v, 60, p. 311-325.
(5) Stoykova, K. and Ivanov, M., 2002. Event and sequence stratigraphy of the Maastrichtian and Danian in Bulgaria. Geologica Balcanica, v. 32(2-4), p.55-62.
(6) Lüning, S., Marzouk, A.M. and Kuss, J., 1998. The Paleocene of central East Sinai, Egypt; sequence stratigraphy in monotonous hemipelagites. The Journal of Foraminiferal Research, v. 28(1), p.19-39.
(7) Farouk, S., 2016. Paleocene stratigraphy in Egypt. Journal of African Earth Sciences, v. 113, p.126-152
(8) Afzal, J., Williams, M. and Aldridge, R.J., 2009. Revised stratigraphy of the lower Cenozoic succession of the Greater Indus Basin in Pakistan. Journal of Micropalaeontology, v. 28(1), p.7-23.
(9) Mitchell, S.M., Beamish, G.W.J., Wood, M.V., Malacek, S.J., Armentrout, J.A., Damuth, J.E. and Olson, H.C., 1993. Paleogene sequence stratigraphic framework of the Faeroe Basin. In Geological Society, London, Petroleum Geology Conference Series, v. 4 (1), p. 1011-1023.
(10) Michelsen, O., Thomsen, E., Danielsen, M., Heilmann-Clausen, C., Jordt, H., Laursen, G.V. and De Graciansky, P.C., 1998. Cenozoic sequence stratigraphy in the Eastern North Sea. SEPM Special Publications, v, 60, p. 91-118.
(11) McGowran, B., Holdgate, G.R., Li, Q. and Gallagher, S.J., 2004. Cenozoic stratigraphic succession in southeastern Australia. Australian Journal of Earth Sciences, v. 51(4), p.459-496.
(12) Higgs, K.E., King, P.R., Raine, J.I., Sykes, R., Browne, G.H., Crouch, E.M. and Baur, J.R., 2012. Sequence stratigraphy and controls on reservoir sandstone distribution in an Eocene marginal marine-coastal plain fairway, Taranaki Basin, New Zealand. Marine and Petroleum Geology, v, 32(1), p.110-137.
(13) Miller, K.G., Mountain, G.S., Browning, J.V., Kominz, M., Sugarman, P.J., Christie-Blinck, N., Katz, M.E. and Wright, J.D., 1998. Cenozoic global sea level, sequences, and the New Jersey transect: results from coastal plain and continental slope drilling. Reviews of Geophysics, v. 36(4), p.569-601.
(14) Vakarcs, G., Hardenbol, J., Abreu, V.S., Vail, P.R., Várnai, P. and Tari, G., 1998. Oligocene-Middle Miocene depositional sequences of the central Paratethys and their correlation with regional stages. Special Publications SEPM, v, 60, p. 209-232.

(15) Ameen Lawa, F.A. and Ghafur, A.A., 2015. Sequence stratigraphy and biostratigraphy of the prolific late Eocene, Oligocene and early Miocene carbonates from Zagros fold-thrust belt in Kurdistan region. Arabian Journal of Geosciences, v. 8, p. 8143-8174.
(16) Gnaccolini, M., Gelati, R., Falletti, P., Catrullo, D. and de Graciansky, P.C., 1998. Sequence Stratigraphy of the" Langhe" Oligo-Miocene Succession, Tertiary Piedmont Basin Northern Italy. SEPM Special Publications, v, 60, p.233-244.
(17) Coffey, B.P. and Read, J.F., 2007. Subtropical to temperate facies from a transition zone, mixed carbonat-siliciclastic system, Palaeogene, North Carolin, USA, Sedimentology, v. 54(2), p.339-365.
(18) Eberli, G.P. and Ginsburg, R.N., 1989. Cenozoic progradation of northwestern Great Bahama Bank, a record of lateral platform growth and sea-level fluctuations. SEPM special publication, v. 4, p. 339-351.
(19) Bartek, L.R., Henrys, S.A., Anderson, J.B. and Barrett, P.J., 1996. Seismic stratigraphy of McMurdo Sound, Antarctica: implications for glacially influenced early Cenozoic eustatic change. Marine Geology, v. 130(1-2), p.79-98.
(20) Hentz, T.F. and Zeng, H., 2003. High-frequency Miocene sequence stratigraphy, offshore Louisiana: Cycle framework and influence on production distribution in a mature shelf province. AAPG Bulletin, v. 87(2), p.197-230.
(21) Sørensen, J.C. and Michelsen, O., 1995. Upper Cenozoic sequences in the southeastern north sea basin. Bulletin of the Geological Society of Denmark, v. 42(1), p.74-95.
(22) Krézsek, C. S., and Filipescu, S., 2005. "Middle to late Miocene sequence stratigraphy of the Transylvanian Basin (Romania)." Tectonophysics, v. 410(1-4), p. 437-463.
(23) Gorini, C., Haq, B.U., dos Reis, A.T., Silva, C.G., Cruz, A., Soares, E. and Grangeon, D., 2014. Late Neogene sequence stratigraphic evolution of the Foz do Amazonas Basin, Brazil. Terra Nova, v. 26(3), p.179-185.
(24) Catalano, R., Di Stefano, E., Sulli, A., Vitale, F.P., Infuso, S. and Vail, P.R., 1998. Sequences and Systems Tracts Calibrated by High Resolution Bio-Chronostratigraphy: The Central Mediterranean Plio-Pleistocene Record SEPM Special Publications, v, 60, p. 155-178.
(25) Lu, H. and Fulthorpe, C.S., 2004. Controls on sequence stratigraphy of a middle Miocene–Holocene, current-swept, passive margin: offshore Canterbury Basin, New Zealand. Geological Society of America Bulletin, v. 116(11-12), p.1345-1366.
(26) Rise, L., Ottesen, D., Berg, K. and Lundin, E., 2005. Large-scale development of the mid-Norwegian margin during the last 3 million years. Marine and Petroleum Geology, v. 22(1-2), p.33-44.
(27) Hafeez, A., 2011. Late Cenozoic sedimentary outbuilding offshore Mid-Norway: A sequence stratigraphic analysis (Master's thesis available online).
(28) Alexandropoulou, N., 2013. Late Cenozoic evolution of the upper Bjørnøya Fan, western Barents Sea margin: A seismic sequence stratigraphic analysis (Master's thesis available online).

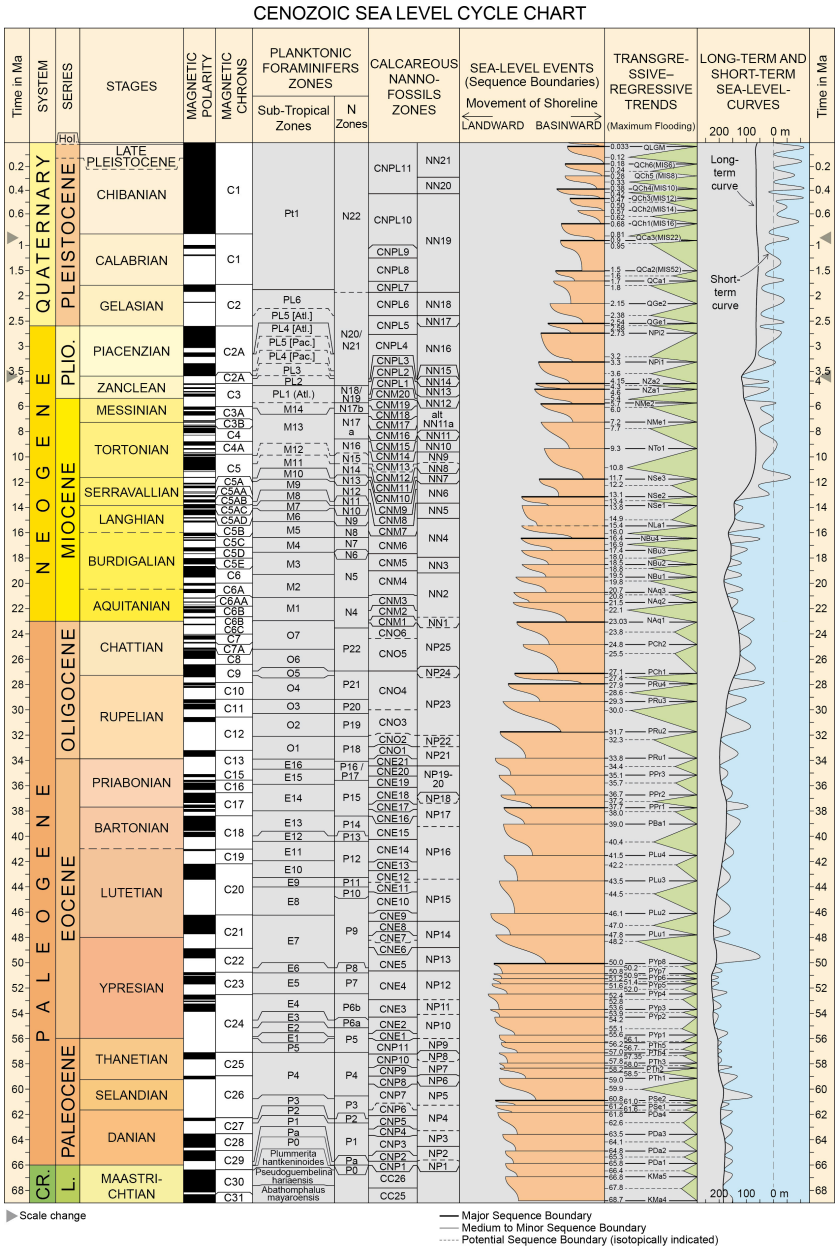

Figure S1. Composite Cenozoic depositional sequences and eustatic sea-level variations. Columns from left to right include: numerical time scale, magnetostratigraphy and biostratigraphic zones after various authors (GTS 2020, see, Speijer et al, 2020, Raffi et al., 2020 and Gibbard and Head, 2020, for details). Sea-level fall events (sequence boundaries) are labeled with unique alphanumeric designations (third column from right), where first letters "P" , "N" or "Q" stand for is for Paleogene, Neogene and Quaternary, respectively, followed by two first letters of the Stage name and a number to identify the oldest to youngest event in that Stage. Also listed in this column, the ages of the sequence boundaries and MFSs that are fine-tuned by calibrations with oxygen-isotopic data (after Westerhold et al., 2020). For the Quaternary sequences, 1.5 Ma and younger, Marine Isotope Stage numbers (e.g., MIS22) in which the SBs occur are also added. The youngest SB that occurred at the time of the Last Glacial Maximum is designated as QLGM. [Note the scale changes at 3.6 and 1.8 Ma in the numerical time scale columns].